Accepted Manuscript

Crystal structure, Raman spectroscopy and microwave dielectric properties of $Li_{1+x}ZnNbO_4$ ($0 \leq x \leq 0.05$) ceramics

Yunfei Tian, Ying Tang, Kai Xiao, Chunchun Li, Lian Duan, Liang Fang

PII: S0925-8388(18)33132-3

DOI: 10.1016/j.jallcom.2018.08.244

Reference: JALCOM 47332

To appear in: *Journal of Alloys and Compounds*

Received Date: 21 May 2018

Revised Date: 11 August 2018

Accepted Date: 25 August 2018

Please cite this article as: Y. Tian, Y. Tang, K. Xiao, C. Li, L. Duan, L. Fang, Crystal structure, Raman spectroscopy and microwave dielectric properties of $Li_{1+x}ZnNbO_4$ ($0 \leq x \leq 0.05$) ceramics, *Journal of Alloys and Compounds* (2018), doi: 10.1016/j.jallcom.2018.08.244.

Crystal structure, Raman Spectroscopy and Microwave Dielectric Properties of $Li_{1+x}ZnNbO_4$ ($0 \leq x \leq 0.05$) Ceramics

Yunfei Tian[1, 2], Ying Tang[1*], Kai Xiao[1], Chunchun Li[1], Lian Duan[1], Liang Fang[1, 2*]

[1]*State Key Laboratory Breeding Base of Nonferrous metals and specific Materials Processing, Guangxi universities key laboratory of non-ferrous metal oxide electronic functional materials and devices, College of Material Science and Engineering, Guilin University of Technology, Guilin, 541004, China*

[2] *Key laboratory of inorganic nonmetallic crystalline and energy conversion materials, College of Materials and Chemical Engineering, Three Gorges University, Yichang, 443002, China*

Abstract

A series of $Li_{1+x}ZnNbO_4$ ($0 \leq x \leq 0.05$) spinel-structured ceramics were prepared by the conventional solid-state reaction. The phase composition，microstructure and relationship between the structure and microwave dielectric properties were investigated using X-ray diffraction, Raman spectroscopy, and scanning electron microscope. When x = 0.02, the outstanding microwave dielectric properties of $Li_{1+x}ZnNbO_4$ ($0 \leq x \leq 0.05$) ceramics were achieved with ε_r = 14.9, $Q \times f$ = 104,600 GHz (at 9 GHz), and τ_f = -64.0 ppm/^{o}C. The dielectric constant and $Q \times f$ value decreased with the increase of Raman shift and FWHM of the A_{1g} mode. Furthermore, the large negative τ_f of $Li_{1+x}ZnNbO_4$ ($0 \leq x \leq 0.05$) ceramics could be modified by adding $CaTiO_3$, and the $0.92Li_{1.02}ZnNbO_4$-$0.08CaTiO_3$ ceramic sintered at 1120 ^{o}C for 4 h exhibited a near-zero τ_f value of -1.4 ppm/^{o}C along with a ε_r of 21.3 and a $Q \times f$ value of 92,500 GHz.

Keywords: Structure refinement; Raman spectroscopy; Microwave dielectric properties; Spinel structure

* Corresponding Author, tangyinggl001@aliyun.com; fanglianggl001@aliyun.com;

1. Introduction

With the development of wireless communication, microwave dielectric ceramics as the microwave integrated circuits (MIC) of key materials have aroused the wide attention of scientists and consequently gained rapid development in the past several decades [1-3]. It is well known that three figure-of-merits are required for actual applications, namely, an appropriate permittivity (ε_r), a high quality factor ($Q \times f$), and a near-zero temperature coefficient of resonance frequency (τ_f) for temperature stability [4,5]. Nowadays, the search for high Q factor becomes one of the most popular researches in the field of dielectrics, because of their potential applications in microwave substrates, filters, and resonators [6]. The materials with a high Q factor can provide better frequency control accuracy and a higher frequency response steepness of the passband edge signal. These characteristics are conducive to the suppression of electronic noise, reduce signal crosstalk and improve the frequency band utilization in the circuit, which is the key requirement for modern wireless practical applications [7].

Recently the spinel compounds with a general formula AB_2O_4 have been extensively investigated due to their excellent mechanical and dielectric performances [8]. Some Li-containing spinels were reported to be promising microwave dielectric materials due to their excellent dielectric performances and relatively low sintering temperature, such as $Li_2MTi_3O_8$ (M=Zn, Mg, Co), $Li_2M_3Ti_4O_{12}$ (M=Zn, Mg) and $Li_4Ti_5O_{12}$ [9-13]. The crystal structure of spinel $LiZnNbO_4$ was first reported by González, with tetrahedral sites occupied by Zn and 1:1 cation ordering of Li and Nb at octahedral sites [14]. Pang et al. reported that the $LiZnNbO_4$ ceramic could be well densified at around 950 ^oC and possessed of good microwave dielectric performances

with $\varepsilon_r \sim 14.6$, $Q \times f \sim 47{,}200$ GHz, and $\tau_f \sim -64.5$ ppm/^{o}C [15]. Zhou et al. further improved the microwave dielectric performance $LiZnNbO_4$ up to $\varepsilon_r \sim 15.6$, $Q \times f \sim$ 85,310 GHz, and $\tau_f \sim -63.7$ ppm/^{o}C via the pretreatment of raw materials [16], but its sintering temperature was 1070 ^{o}C, which is rather higher compared to the previous reports. In addition, many researches have reported that the microwave dielectric properties of some Li-containing ceramics could be dramatically enhanced by the slight excess of Li effects, such as the $Li_{2+x}TiO_3$ ($0 \le x \le 0.2$), $Li_{4+x}Ti_5O_{12}$ ($0 \le x \le 1.2$) and $Li_2Zn_{1-x}Ge_3O_8$ ($0 \le x \le 0.2$) [17-19]. This inspires us to study the effect of Li excess on the structure and microwave dielectric properties in $LiZnNbO_4$ ceramics. So that a series of $Li_{1+x}ZnNbO_4$ ($0 \le x \le 0.05$) spinel ceramics were prepared in this work, and their sintering behavior, crystal structure, Raman spectroscopy, and microwave dielectric properties were investigated. The temperature stability was also enhanced by doping $CaTiO_3$ to form composite ceramics.

2. Experimental procedures

Samples of $LiZnNbO_4$ with different Li-contents were prepared via a conventional mixed-oxide route. The compositions can be described as $Li_{1+x}ZnNbO_4$ with x = 0, 0.01, 0.02, 0.03, 0.04, 0.05. As starting materials for the synthesis Li_2O (99.99%), ZnO (99.99%), Nb_2O_5 (99.99%) were used. These raw powders were weighted and balled firstly in a polyamide jar for 24 h with ZrO_2 balls using the ethanol as dispersants after mixing, then the slurries were dried at 120 ^{o}C. For the purpose of binding of Li component, calcined preliminarily at 500 ^{o}C for 10 h and then sintered at 900 ^{o}C for 2 h at a heating rate of 5 ^{o}C/min. Subsequently, the material was again ball milled using the same milling parameters as in the first milling step. After dried at 120 ^{o}C, the obtained powders were mixed with 5wt.% polyvinyl alcohol (PVA) solution as a binder, the granulated powders were pressed uniaxially

into the cylinders of 10 mm in diameter and 5 ~ 6 in thickness under a pressure of 200 MPa. Finally, the samples were fired at 600 ^{o}C for 2h to expel the organic binder and then sintered at 1020-1100 ^{o}C for 4 h at a heating rate of 3 ^{o}C/min.

The crystal structures of the ceramics were analyzed by using the X-ray diffraction technique ($CuK_{\alpha 1}$, 1.54059 Å, Model X'Pert PRO, PANalytical, Almelo, Holland). The Raman spectra of the $Li_{1+x}ZnNbO_4$ ceramics were recorded using a DXR Raman Microscope (Thermo Fisher Scientific DXR, America) with a 532 nm line in the range of 100–1000 cm^{-1}. The microstructures of sintered specimens were observed by scanning electron microscope (Model JSM6380-LV SEM, JEOL, Tokyo, Japan). The relative densities of the sintered ceramics were measured by using the Archimedes method. The dielectric constant and quality factor of the samples were measured using a network analyzer (N5230A, Agilent, America) in the frequency range of 10–12 GHz and the temperature coefficient of resonant frequency was obtained by noting the temperature shifts of the resonance scope from room temperature to 85 ^{o}C using a temperature chamber (Delta 9039, Delta Design, San Diego, CA).

3. Results and discussion

Fig. 1 shows X-ray diffraction patterns of $Li_{1+x}ZnNbO_4$ ($0 \leq x \leq 0.05$) ceramics sintered at the optimum temperature for 4 h. In the composition range from 0 to 0.05, all the observed peaks could be indexed based on JCPDS file No. 01-082-1437 for $LiZnNbO_4$, indicating that single phase with a tetragonal spinel structure in space group $P4_322$ was formed when $0 \leq x \leq 0.04$, however, when $x = 0.05$, trace amount of impurity phases were detected near the characteristic peaks of (201) and (210) of the main phase $LiZnNbO_4$. Rietveld refinement of the powder XRD profiles for $Li_{1.02}ZnNbO_4$ ceramic sintered at 1060 ^{o}C/4 h is shown in Fig. 2. The structure that

contains tetrahedral and octahedral groups belongs to a spinel derivative in which the octahedral sites are ordered into two sets with full occupancy by Li and Nb, while the tetrahedral sites are occupied by a disordered Zn. Furthermore, the structural parameters for the $Li_{1+x}ZnNbO_4$ ($0 \leq x \leq 0.05$) ceramic samples in Table 1 were calculated through the least square method based on XRD data and their variations with respect to Li addition content (x value) are shown in Fig. 3, at lower addition range ($x < 0.02$), a nearly linear increase was observed but deviation from linear variation was obtained at higher Li addition ($x > 0.02$). Based on the previous work on Li-containing materials and the Vegard's law [20], which indicates that lower addition range ($x < 0.02$) might enter the crystal structure to form a solid solution.

Fig. 4 demonstrates the secondary electron emission on the polished and thermally etched surfaces of $Li_{1+x}ZnNbO_4$ ceramics. All samples exhibited a dense and uniform microstructure with well-developed grains and identifiable grain boundaries. No obvious change in the grain morphology with increasing x value is observed and the average grain size of the sample with $0 \leq x \leq 0.05$ is in the range of 10-40 μm. As shown in Fig. 4 (d-f), it is noting that some visible pores exist in the grains and the grain boundaries and a small part of the grains are abnormal growth.

Fig. 5(a) shows the relative densities of $Li_{1+x}ZnNbO_4$ ($0 \leq x \leq 0.05$) ceramics as a function of sintering temperature. For all the samples, the relative density is observed to increase initially with the increase of sintering temperature and reaches a maximum at various temperatures depending on the composition. A further increase in the sintering temperature results in a slight decrease in the densification. The $x = 0.02$ exhibited the highest relative density of 97.6% (of the bulk density ~ 4.78 g/cm^3), which coincides with the dense microstructure.

The variation of dielectric permittivity of $Li_{1+x}ZnNbO_4$ ($0 \leq x \leq 0.05$) ceramics with sintering temperature is shown in Fig. 5(b). The dielectric permittivity firstly increased with the increase of sintering temperature and reached a maximum value of 14.9 at $x = 0.02$ composition. The variation of dielectric permittivity is consistent with the change of the relative density. The variation of $Q \times f$ value as a function of sintering temperature is shown in Fig. 5(c). The $Q \times f$ value also obtained its relative optimum values of 104,600 GHz at $x = 0.02$ in the samples with the highest density. It was reported that the $Q \times f$ value was strongly dependent on their densification and the microstructure. Other factors such as grain boundaries, crystal defects, secondary phases, and pores also affect the $Q \times f$ value [21]. In this study, the excess Li with an appropriate level increased densification to more than 95%, so the $Q \times f$ increased firstly with the increasing Li content. But with the further increase of Li content, the $Q \times f$ value decreased sharply due to the appearance of secondary phases and pores. The τ_f value showed a weak dependence on sintering temperature and composition, ranging from −64.0 ppm/^{o}C to −67.2 ppm/^{o}C in Fig. 5(d).

Raman spectroscopy is a more powerful tool than XRD for the detection of local crystal structures, short-range ordering, more specifically cationic occupancy sites, and also provides information that relates vibrational properties to microwave dielectric properties [22]. The room-temperature Raman spectra of the $Li_{1+x}ZnNbO_4$ ($0 \leq x \leq 0.05$) ceramics in the range of 100–1000 cm^{-1} is shown in Fig. 6. Similar Raman spectra were observed for the samples ($0 \leq x \leq 0.05$), however, it is difficult to distinguish the second phase, which might be due to the undetectable amount or the overlapping of the Raman active modes.

The vibration modes near the center of the first Brillouin zone of $LiZnNbO_4$ were characterized using the group theoretical method according to the $P4_322$ space group, as follows [23,24]:

$$\Gamma = 6A_1 + 7B_1 + 8B_2 + 15E \quad \text{(Acoustic modes not included)} \qquad (3)$$

The classification of vibration modes of $LiZnNbO_4$ is listed in Table 2. 22 Gaussia-Lorentzian modes of $Li_{1.02}ZnNbO_4$ are shown in Fig. 7. The bands with wave number greater than 350 cm^{-1} could be associated with several modes involving stretching of cation-O bonds. Since some weak modes were broadened and overlapped, the number of modes observed was smaller than predicted by group-theoretical analysis. According to the report of Aldon et al. [25], the peaks observed at 494 cm^{-1} were assigned to stretching vibration of ZnO_4 tetrahedron. In oxides where lithium is octahedrally coordinated by oxygen, the frequencies of Li-O stretches lie within 250-450 cm^{-1} region [26]. Blasse and van den Heuvel suggest that Nb-O octahedra in cubic Na_3NbO_4 show strong Raman shift at about 800 cm^{-1} [27], then the strong bands centered at 816 cm^{-1} might be assigned to stretching vibration of NbO_6 octahedron. For wavenumbers between 200 cm^{-1} and 350 cm^{-1}, the bands were principally due to bending of O-cation-O. The origin of the bands with wave number below 200 cm^{-1} is lattice vibrations, mainly associated with cations [28].

The stretch mode (A_{1g} with wavenumber around 816 cm^{-1}) of NbO_6 octahedron has the highest frequency and strongest polarity of the vibration modes, exerting the strongest influence on the microwave dielectric properties [29]. Therefore, the Raman shift and FWHM of the A_{1g} mode for $Li_{1+x}ZnNbO_4$ ($0 \leq x \leq 0.05$) ceramics are presented in Table 3. The correlation between the A_{1g} mode and microwave dielectric properties of the $Li_{1+x}ZnNbO_4$ ($0 \leq x \leq 0.05$) ceramic is further discussed. The variation of the dielectric permittivity and the Raman shift of the A_{1g} mode with x is

shown in Fig. 8. The dielectric constant decreased linearly with an increase of the Raman shift of the A_{1g} mode. This can be explained based on the fact that an A_{1g} mode at higher wavenumber corresponds to higher vibration energy and more rigid oxygen octahedron, resulting in lower dielectric constant. The variation of the FWHM also showed the opposite trend compared with the $Q \times f$ value in Fig. 9. This phenomenon is mainly due to the fact that FWHM value of the A_{1g} mode is directly related to the lattice vibration damping coefficient. With the decrease of the FWHM of A_{1g}, the non-harmonic vibrations decrease, which weakens the coherence and damping behavior and reduces the intrinsic dielectric loss [30].

In summary, the sample with x = 0.02 exhibited the optimum microwave dielectric properties with a permittivity of 14.9, a $Q \times f$ value of 104,600 GHz and a τ_f value of -64.0 ppm/^{o}C. Compared with the nominal $LiZnNbO_4$ ceramics (ε_r ~ 14.6, $Q \times f$ ~ 47,200 GHz and τ_f ~ -64.5 ppm/^{o}C), the quality factor is significantly improved. This result indicates that the appropriate addition of excess Li could improve the dielectric performances of $LiZnNbO_4$. However, the large negative τ_f value would impede the practical applications. It is reported that τ_f value can be turned by compositional engineering such as the formation of solid solution or mixtures of dielectrics with opposite τ_f values [31]. In our previous report, near-zero τ_f values could be achieved by compensating the large negative τ_f with rutile TiO_2 or $CaTiO_3$ having positive τ_f values (+465 ppm/^{o}C and +800 ppm/^{o}C, respectively) [32]. Therefore, $CaTiO_3$ was chosen to compensate the τ_f value of $Li_{1.02}ZnNbO_4$ ceramic. A series of composite ceramics in the $(1-x)Li_{1.02}ZnNbO_4$-$xCaTiO_3$ ($0 \le x \le 0.10$) system were prepared. Fig. 10 shows the XRD pattern of the $0.92Li_{1.02}ZnNbO_4$-$0.08CaTiO_3$ ceramic sintered at 1120 ^{o}C for 4 h and XRD patterns of $LiZnNbO_4$ and $CaTiO_3$ are also given for comparison. Only the peaks belonging to $LiZnNbO_4$ and $CaTiO_3$ could

be observed without secondary phase detected, suggesting no chemical reaction between them. In addition, with an increase of x value, the τ_f value obviously increased from -64.0 to -1.4 ppm/^{o}C along with the ε_r increased from 14.9 to 22.5. A near-zero τ_f could be achieved at x = 0.08 with ε_r = 21.3, $Q \times f$ = 92,500 GHz and τ_f = -1.4 ppm/^{o}C in Table 4.

4. Conclusions

In this study, a series of microwave dielectric $Li_{1+x}ZnNbO_4$ ($0 \leq x \leq 0.05$) ceramics with tetragonal spinel structure were prepared by a conventional solid-state reaction method. When x = 0.02, the dense microstructure with a relative density of 97.6%, and the component sintered at 1060 ^{o}C for 4 h achieved excellent microwave dielectric properties with a permittivity of 14.9, a $Q \times f$ value of 104,600 GHz (at 9 GHz), and a negative τ_f value of -64.0 ppm/^{o}C. Moreover, the large negative τ_f of $Li_{1+x}ZnNbO_4$ (x=0.02) ceramic could be modified by adding $CaTiO_3$, and the $0.92Li_{1.02}ZnNbO_4$-$0.08CaTiO_3$ ceramic sintered at 1120 ^{o}C for 4 h exhibited favorable dielectric properties with a ε_r of 21.3, a $Q \times f$ value of 92,500 GHz and a near-zero τ_f value of -1.4 ppm/^{o}C.

References

[1] J.C. Kim, M.H. Kim, S. Nahm, J.H. Paik, J.H. Kim, H.J. Lee, Microwave dielectric properties of $Re_3Ga_5O_{12}$ (Re: Nd, Sm, Eu, Dy and Yb) ceramics and effect of TiO_2 on the microwave dielectric properties of $Sm_3Ga_5O_{12}$ ceramics, J. Eur. Ceram. Soc. 27 (2007) 2865-2870.

[2] C.C. Li, H.C. Xiang, M.Y. Xu, Y. Tang, L. Fang, Li_2AGeO_4 (A=Zn, Mg): Two novel low permittivity microwave dielectric ceramics with olivine structure. J. Eur. Ceram. Soc. 38 (2018) 1524-1528.

[3] C.C. Li, H.C. Xiang, Y. Tang, M.Y. Xu, J. Khaliq, J.Q. Chen, L. Fang, Low firing and temperature stable microwave dielectric ceramics $Ba_2LnV_3O_{11}$ (Ln=Nd, Sm), J. Am. Ceram. Soc. 101 (2018) 773-781.

[4] M.T. Sebastian, Dielectric materials for wireless communication, Elsevier. Oxford. UK. 2010.

[5] T. Teranishi, R. Kanemoto, H. Hayashi, A. Kishimoto, Effect of the (Ba + Sr)/Ti ratio on the microwave-tunable properties of $Ba_{0.6}Sr_{0.4}TiO_3$ ceramics, J. Am. Ceram. Soc. 100 (2017) 1037-1043.

[6] J.X. Bi, C.C. Li, Y.H. Zhang, C.F. Xing, C.H. Yang, H.T. Wu, Crystal structure, infrared spectra and microwave dielectric properties of ultra low-loss $Li_2Mg_4TiO_7$ ceramics, Mater. Lett. 196 (2017) 128–131.

[7] W. Lei, W.Z. Lu, J.H. Zhu, F. Liang, D. Liu, Modification of $ZnAl_2O_4$-based low permittivity microwave dielectric ceramics by adding 2MO-TiO_2 (M=Co, Mg, and Mn), J. Am. Ceram. Soc. 91 (2008) 1958-1961.

[8] R.W. Grimes, A.B. Anderson, A.H. Heuer, Predictions of cation distributions in AB_2O_4 spinels from normalized ion energies, J. Am. Chem. Soc. 111 (1989) 1-7.

[9] S. George, S.M. Sebastian, Synthesis and microwave dielectric properties of

novel temperature stable high Q $Li_2ATi_3O_8$ (A=Mg, Zn) ceramics, J. Eur. Ceram. Soc. 30 (2010) 2585-2592.

[10] L. Fang, D.J. Chu, H.F. Zhou, X.L. Chen, Z. Yang, Microwave dielectric properties and low temperature sintering behavior of $Li_2CoTi_3O_8$ ceramic, J. Alloy. Compd. 509 (2011) 1880-1884.

[11] H.F. Zhou, X.H. Tan, J. Huang, X.L. Chen, Sintering behavior, phase evolution and microwave dielectric properties of thermally stable Li_2O-3MgO-$mTiO_2$ ceramics ($1 \leq m \leq 6$), Ceram. Int. 43 (2016) 3688-3692.

[12] H.S. Ren, S.H. Jiang, M.Z. Dang, T.Y. Xie, H. Tang, H.Y. Peng, H.X. Lin, L. Luo, Investigating on sintering mechanism and adjustable dielectric properties of BLMT glass/$Li_2Zn_3Ti_4O_{12}$ composites for LTCC applications, J. Alloy. Compd. 740 (2018) 1188-1196.

[13] J. Zhang, R.Z. Zuo, Y. Wang, S.S. Qi, Phase evolution and microwave dielectric properties of $Li_4Ti_{5(1+x)}O_{12}$ ceramics, Mater. Lett. 164 (2016) 353-355.

[14] C. González, M.L. López, M. Gaitán, M.L. Veiga, C. Pico, Relationship between crystal structure and electric properties for lithium-containing spinels, Mater. Res. Bullet. 29 (1994) 903-910.

[15] L.X. Pang, D. Zhou, A low-firing microwave dielectric material in Li_2O-ZnO-Nb_2O_5 system, Mater. Lett. 64 (2010) 2413-2415.

[16] H.F. Zhou, J.Z. Gong, G.C. Fan, X.L. Chen, Enhanced sintering ability and microwave dielectric properties of $LiZnNbO_4$ ceramics with pretreatment of raw materials, J. Alloy. Compd. 665 (2016) 113-118.

[17] J.J. Bian, Y.F. Dong, Sintering behavior, microstructure and microwave dielectric properties of $Li_{2+x}TiO_3$ ($0 \leq x \leq 0.2$), Mater. Sci. Eng. B. 176 (2011) 147-151.

[18] W. Li, L. Fang, Y. Tang, Y.H. Sun, C.C. Li, Microwave dielectric properties in the

$Li_{4+x}Ti_5O_{12}$ ($0 \leq x \leq 1.2$) ceramics, J. Alloy. Compd. 701 (2017) 295-300.

[19] H.C. Xiang, L. Fang, Y. Tang, C.C. Li, Effects of Zn non-stoichiometry on the phase evolution and microwave dielectric properties of $Li_2Zn_{1-x}Ge_3O_8$ ($0 \leq x \leq 0.2$) spinels, J. Mater. Sci. 28 (2017) 15605-15611.

[20] L. Zhang, S.C. Li, Empirical atom model of Vegard's law, J. Phys. B. 434 (2014) 38–43.

[21] L Fang, D.J. Chu, H.F. Zhou, X.L. Chen, H. Zhang, B.C. Chang, C.C. Li, Y.D. Qin, X. Huang, Microwave dielectric properties of temperature stable $Li_2Zn_xCo_{1-x}Ti_3O_8$ ceramics, J. Alloy. Compd. 509 (2011) 8840-8844.

[22] H. Luo, L. Fang, H.C. Xiang, Y. Tang, C.C. Li, Two novel low-firing germanates $Li_2MGe_3O_8$ (M = Ni, Co) microwave dielectric ceramics with spinel structure, Ceram. Int. 43 (2017) 1622-1627.

[23] D.L. Rousseau, R.P. Bauman, S.P.S. Porto, Normal mode determination in crystals, J. Raman Spectrosc. 10 (2010) 253-290.

[24] V.L. Gurevich, A.K. Tagantsev, Intrinsic dielectric loss in crystals, Adv. Phys. 40 (1991) 719-767.

[25] L. Aldon, P. Kubiak, M. Womes, J.C. Jumas, J. Olivier-Fourcade, J.L. Tirado, J.I. Corredor, C.P. Vicente, Chemical and electrochemical Li-insertion into the $Li_4Ti_5O_{12}$ spinel, Chem. Mater. 16 (2004) 5721-5725.

[26] T.A. Denisova, L.G. Maksimova, E.V. Polyakov, Metatitanic acid: synthesis and properties, Russ. J. Inorg. Chem. 51 (2006) 691-699.

[27] G. Blasse, G.P.M. V.D. Heuvel, Vibration and electronic spectra and crystal structure of cubic Na_3NbO_4, Mater. Res. Bull. 7 (1972) 1041-1043.

[28] X.P. Lu, Y. Zheng, Q. Huang, Z.W. Dong, Structural dependence of microwave dielectric properties of spinel-structured $Li_2ZnTi_3O_8$ ceramic: crystal structure

refinement and Raman spectroscopy study, J. Electron. Mater. 45 (2016) 940-94.

[29] Y.D. Dai, G.H. Zhao, H.X. Liu, First-principles study of the dielectric properties of $Ba(Zn_{1/3}Nb_{2/3})O_3$ and $Ba(Mg_{1/3}Nb_{2/3})O_3$, J. Appl. Phys. 105 (2009) 421-429.

[30] H.F. Zhou, X.L. Chen, L. Fang, A new low-loss microwave dielectric ceramic for low temperature cofired ceramic applications, J. Mater. Res. 25 (2010) 1235-1238.

[31] L. Fang, D.J. Chu, C.C. Li, H.F. Zhou, Z. Yang, Effect of $BaCu(B_2O_5)$ addition on phase transition, sintering temperature, and microwave dielectric properties of $Ba_4LiNb_3O_{12}$ ceramics, J. Am. Ceram. Soc. 94 (2011) 524-528.

[32] H.C. Xiang, X.W. Jiang, L. Fang, Z.H. Wei, C.C. Li, Microwave dielectric properties of temperature stable $(1-x)BaCaV_2O_7$-$xTiO_2$ composite ceramics, J. Mater. Sci. - Mater. Electron. 26 (2015) 9134-9138.

Table 1. The structural parameters of $Li_{1+x}ZnNbO_4$ ($0 \leq x \leq 0.05$) sintered at 1060 ^oC for 4h.

x	a=b(Å)	c(Å)	V (Å^3)
x = 0	6.0773	8.3658	308.9765
x = 0.01	6.0783	8.3790	309.5723
x = 0.02	6.0816	8.4022	310.7622
x = 0.03	6.0869	8.3959	310.9335
x = 0.04	6.0869	8.3959	310.9334
x = 0.05	6.0814	8.4178	311.3193

Table 2. The classification of vibration mode of $LiZnNbO_4$.

Atom	Site	A_1	A_2	B_1	B_1	E
Li	4a	1	-	1	2	3
Zn	4c	1	-	2	1	3
Nb	4b	1	-	1	2	3
O	8d	3	-	3	3	6
Total		6	-	7	8	15

Table 3. Raman shift and FWHM of A_{1g} mode for $LiZnNbO_4$ ceramic.

Ceramic composition	Raman shift (cm^{-1})	FWHM (cm^{-1})
$LiZnNbO_4$	816.07	20.78
$Li_{1.01}ZnNbO_4$	815.93	20.32
$Li_{1.02}ZnNbO_4$	815.70	18.06
$Li_{1.03}ZnNbO_4$	816.00	20.55
$Li_{1.04}ZnNbO_4$	816.11	20.95
$Li_{1.05}ZnNbO_4$	816.23	21.63

Table 4. Microwave dielectric properties of (1-x)$Li_{1.02}ZnNbO_4$–$xCaTiO_3$ ($0 \leq x \leq 0.10$) ceramics.

x	S.T. (^oC)	ε_r	$Q \times f$ (GHz)	τ_f (ppm/^oC)
0	1060	14.9±0.03	104,600±2000	-64.0±1.8
0.04	1080	18.2±0.04	100,875±1900	-35.4±1.2
0.06	1100	20.6±0.04	96,080±2000	-17.2±0.7
0.08	1120	21.3±0.03	92,500±2100	-1.4±0.3
0.10	1140	22.5±0.04	88,540±2200	12.4±0.5

Figure Captions:

Fig. 1. X-ray diffraction patterns of $Li_{1+x}ZnNbO_4$ ($0 \le x \le 0.05$) ceramics sintered at the optimum temperature for 4 h.

Fig. 2. Observed, calculated and difference powder XRD profiles for $Li_{1.02}ZnNbO_4$ ceramic sintered at 1060 ^oC for 4 h. Insets are lattice structure of the $Li_{1.02}ZnNbO_4$ ceramic.

Fig. 3. The variation of the cell parameters and the cell volume of $Li_{1+x}ZnNbO_4$ ($0 \le x \le 0.5$) ceramics about the x value.

Fig. 4. Scanning electron micrographs of (a) $LiZnNbO_4$ at 1080 ^oC, (b) $Li_{1.01}ZnNbO_4$ at 1060 ^oC, (c) $Li_{1.02}ZnNbO_4$ at 1060 ^oC, (d) $Li_{1.03}ZnNbO_4$ at 1060 ^oC, (e) $Li_{1.04}ZnNbO_4$ at 1040 ^oC, (f) $Li_{1.05}ZnNbO_4$ at 1040 ^oC.

Fig. 5. The variation of relative density and microwave dielectric properties (ε_r, $Q \times f$, and τ_f) of $Li_{1+x}ZnNbO_4$ ($0 \le x \le 0.5$) ceramics as a function of sintering temperature.

Fig. 6. Raman spectra of $Li_{1+x}ZnNbO_4$ ($0 \le x \le 0.5$) ceramics sintered at the optimum temperature.

Fig. 7. Raman Gaussia-Lorentzian fitting of $Li_{1.02}ZnNbO_4$ ceramic.

Fig. 8. Dielectric constant and A_{1g} Raman shift of $Li_{1+x}ZnNbO_4$ ($0 \le x \le 0.05$) ceramic sintered at the optimum temperature for 4 h.

Fig. 9. $Q \times f$ value and A_{1g} FWHM of $Li_{1+x}ZnNbO_4$ ($0 \le x \le 0.05$) ceramic sintered at the optimum temperature for 4 h.

Fig. 10. X-ray diffraction patterns of $0.92Li_{1.02}ZnNbO_4$–$0.08CaTiO_3$ ceramics sintered at 1120 ^oC for 4 h in air.

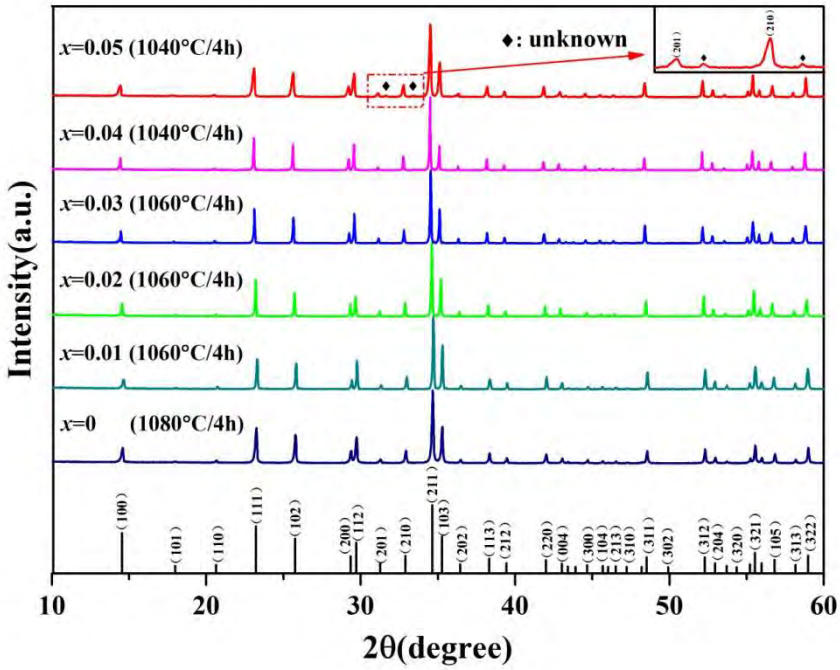

Fig. 1

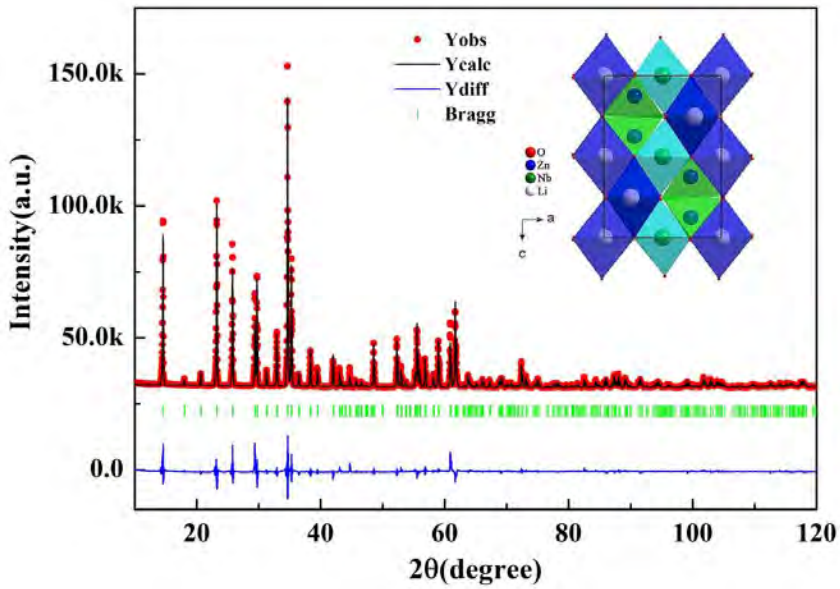

Fig. 2

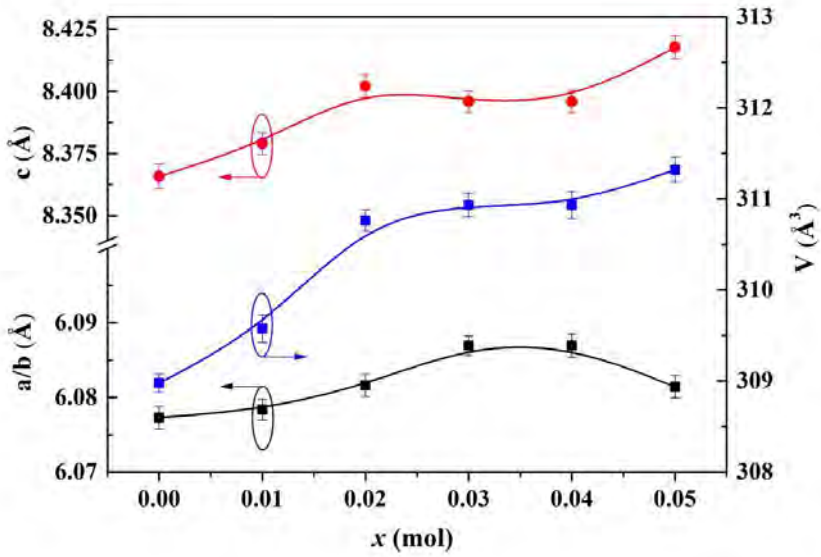
8.425
8.400
8.375
8.350
c (Å)
6.09
6.08
6.07
a/b (Å)
313
312
311
310
309
308
V (Å³)
0.00
0.01
0.02
0.03
0.04
0.05
x (mol)

Fig. 3

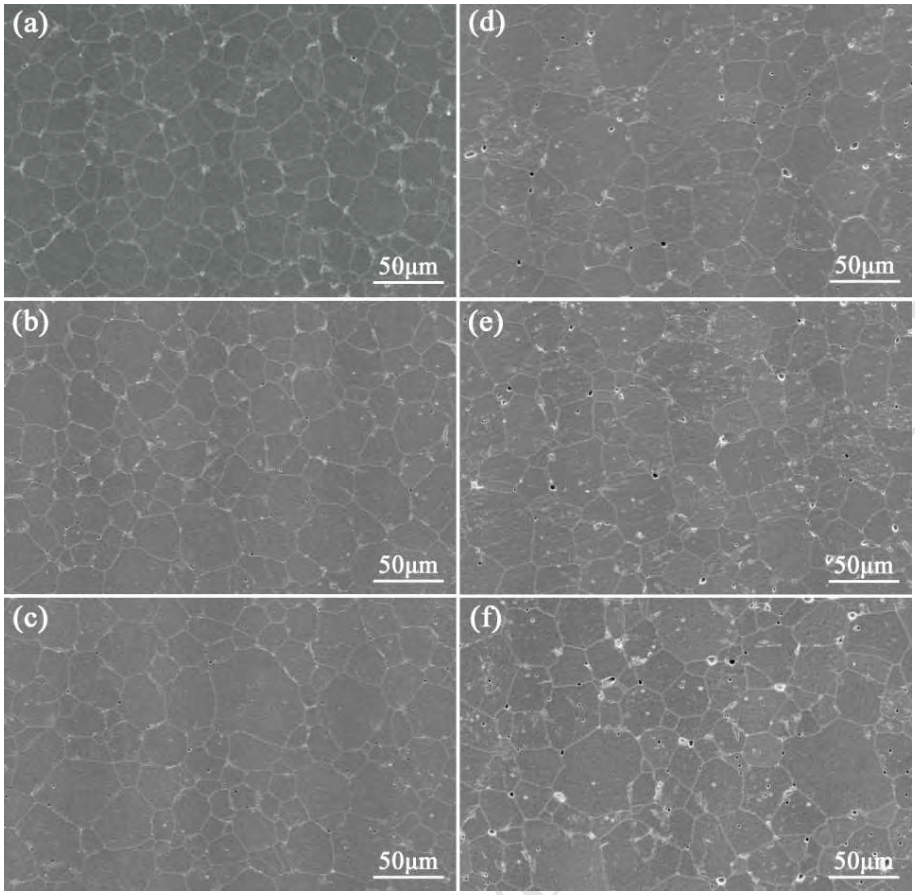

Fig. 4

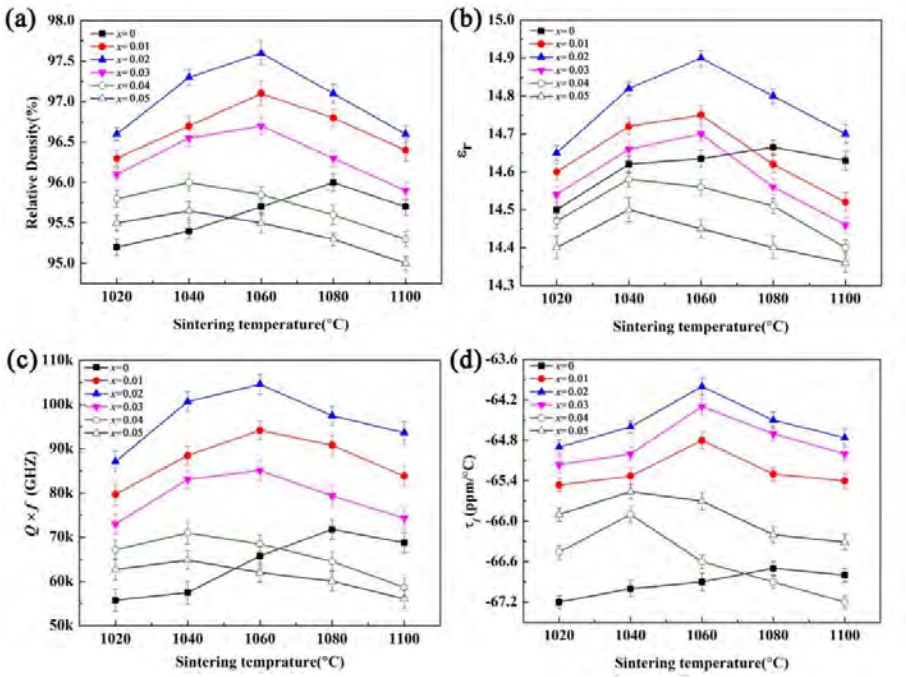

Fig. 5

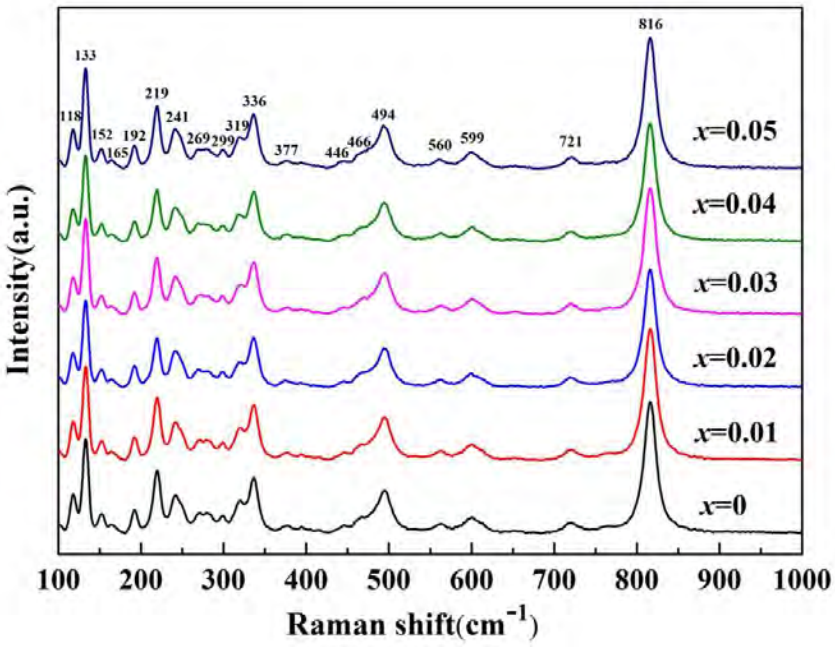

Fig. 6

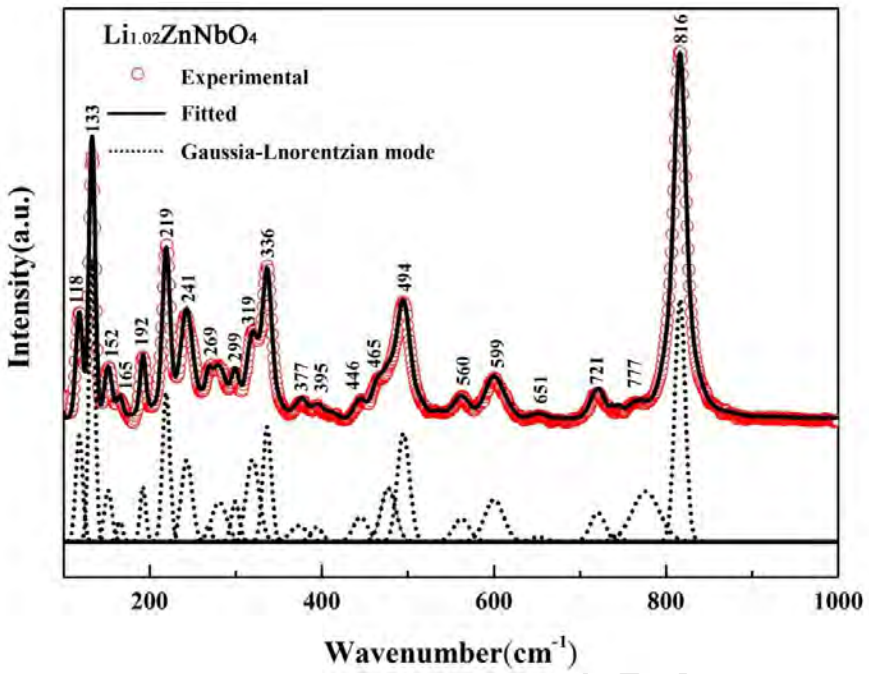

Fig. 7

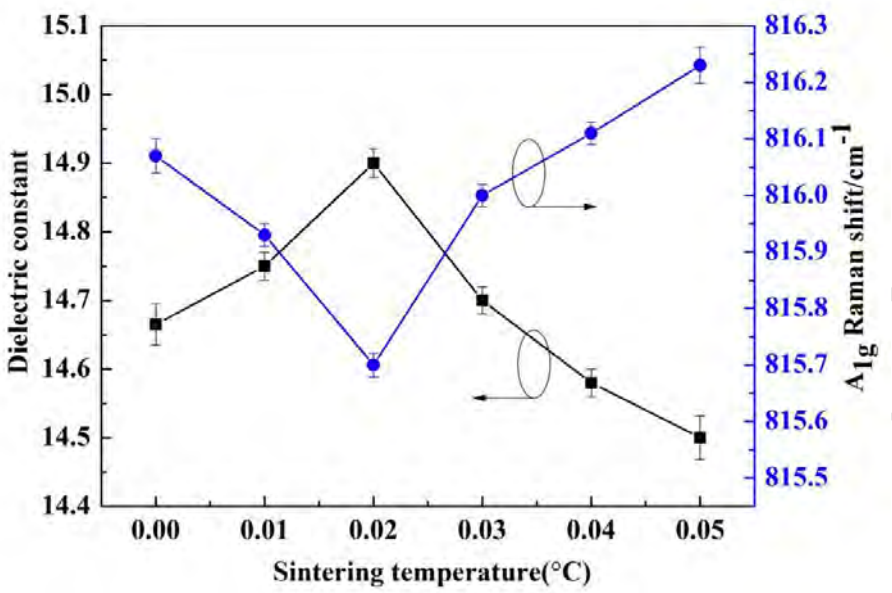

Fig. 8

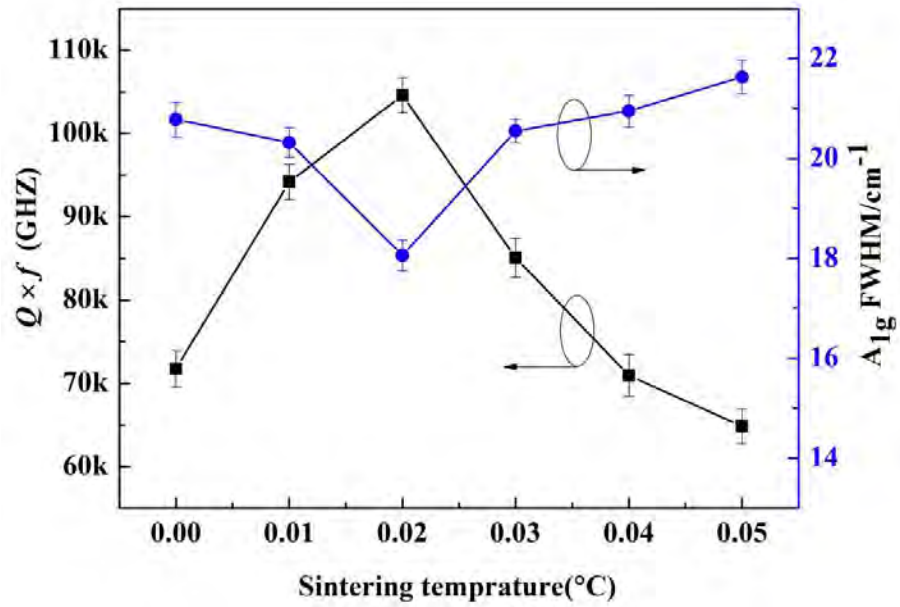

Fig. 9

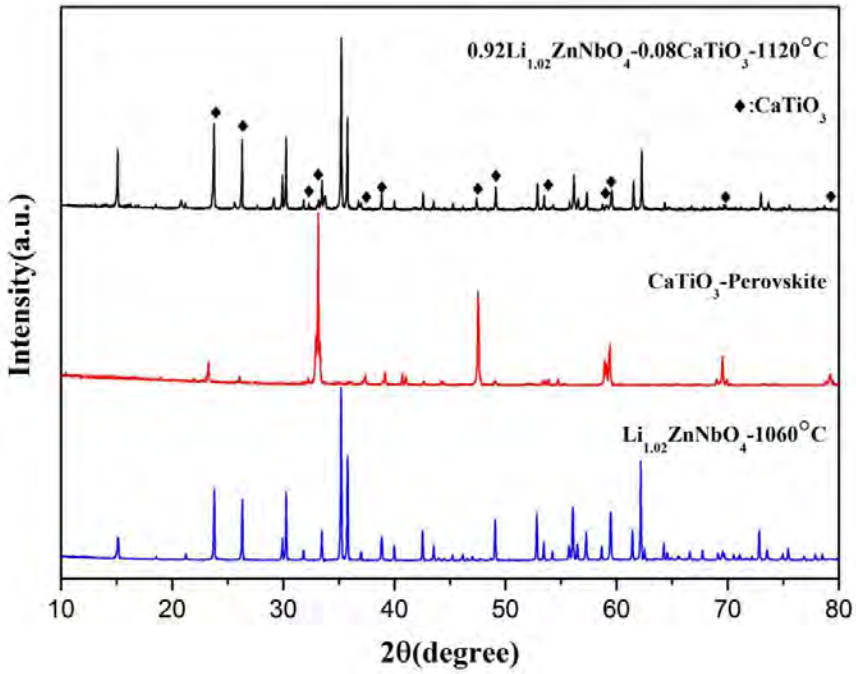

Fig. 10